

UC San Diego

UC San Diego Previously Published Works

Title

Conformationally Gated Electron Transfer in Nitrogenase. Isolation, Purification, and Characterization of Nitrogenase From *Gluconacetobacter diazotrophicus*

Permalink

<https://escholarship.org/uc/item/8vm3w876>

Authors

Owens, Cedric P
Tezcan, Faik A

Publication Date

2018

DOI

10.1016/bs.mie.2017.09.007

Peer reviewed



Published in final edited form as:

Methods Enzymol. 2018 ; 599: 355–386. doi:10.1016/bs.mie.2017.09.007.

Conformationally gated electron transfer in nitrogenase. Isolation, purification and characterization of nitrogenase from *Gluconacetobacter diazotrophicus*

Cedric P. Owens* and F. Akif Tezcan†,1

*Schmid College of Science and Technology, Chapman University, Orange, California, USA

†Department of Chemistry and Biochemistry, University of California, San Diego, La Jolla, California, USA

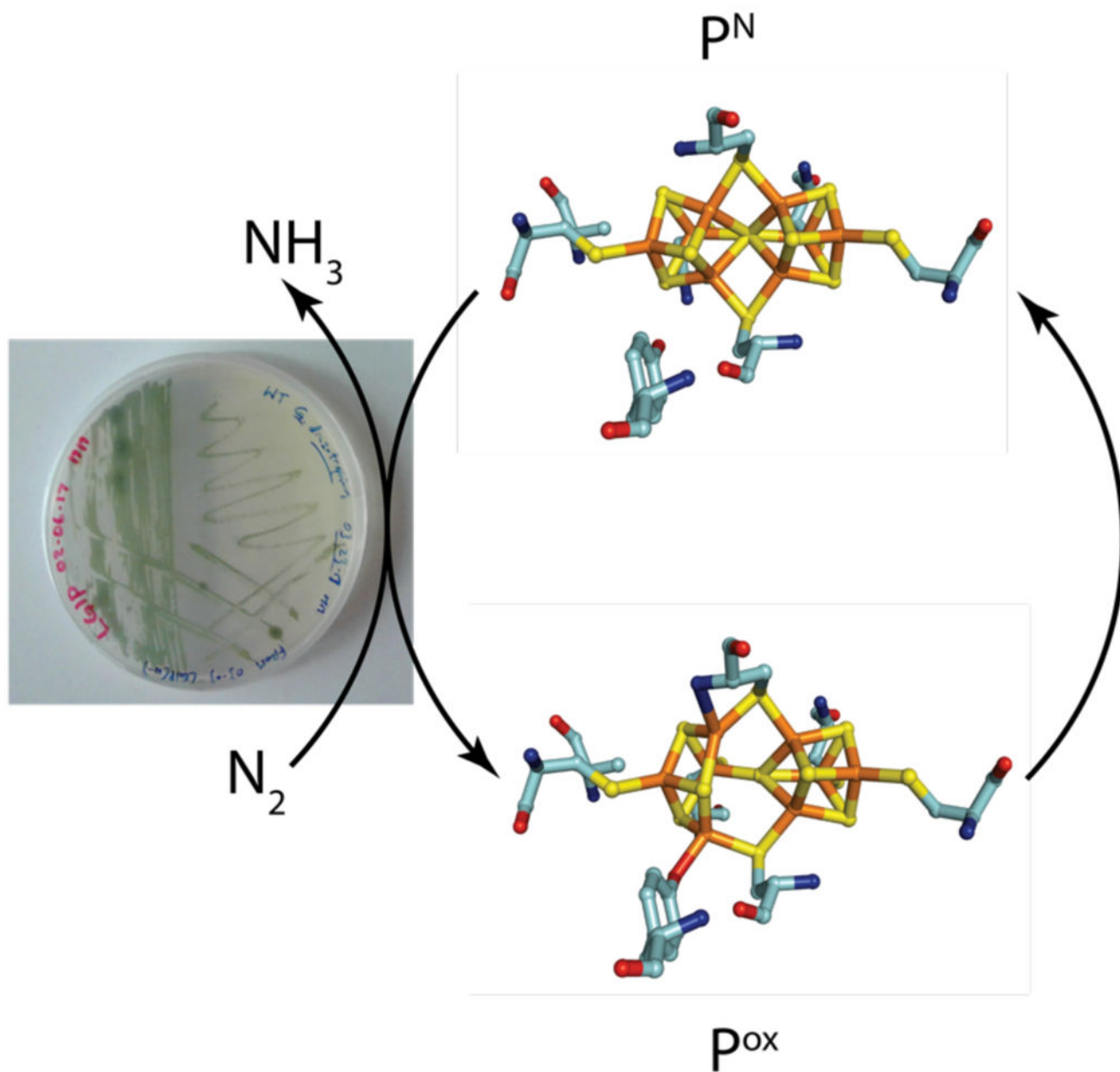
Abstract

Nitrogenase is a complex, bacterial enzyme that catalyzes the ATP-dependent reduction of dinitrogen (N_2) to ammonia (NH_3). It consists of two proteins, the catalytic molybdenum-iron protein (MoFeP) and its specific reductase, the iron protein (FeP). A defining feature of nitrogenase is that electron and proton transfer processes linked to substrate reduction are synchronized by conformational changes driven by ATP-dependent FeP-MoFeP interactions. Yet, despite extensive crystallographic, spectroscopic and biochemical information on nitrogenase, the structural basis of the ATP-dependent synchronization mechanism is not understood in detail. In this chapter, we summarize some of our efforts towards obtaining such an understanding.

Experimental investigations of the structure-function relationships nitrogenase are challenged by the fact that it cannot be readily expressed heterologously in non-diazotrophic bacteria, and the purification protocols for nitrogenase are only known for a small number of diazotrophic organisms. Here, we also present methods for purifying and characterizing nitrogenase from a new model organism, *Gluconacetobacter diazotrophicus*. We also describe procedures for observing redox-dependent conformational changes in *G. diazotrophicus* nitrogenase by X-ray crystallography and electron paramagnetic resonance (EPR) spectroscopy, which have provided new insights into the redox-dependent conformational gating processes in nitrogenase.

Table of Contents Figure

¹corresponding author cpowens@chapman.edu and tezcan@ucsd.edu.



Keywords

Nitrogenase; electron transfer; conformational gating; *Gluconacetobacter diazotrophicus*; P-cluster; protein crystallography; electron paramagnetic resonance

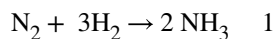
1. Introduction

1.1 Biological and abiological nitrogen fixation

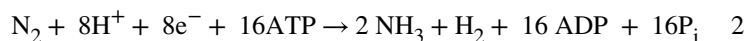
Conversion of atmospheric N_2 into biologically usable NH_3 is necessary for life on earth. Developing methods for enhancing plant NH_3 supply is critical for agriculture since lack of

fixed nitrogen, such as NH₃, often limits crop growth [41, 51]. The two most important sources of NH₃ are biological nitrogen fixation by the enzyme nitrogenase and synthetic nitrogen fixation via the Haber-Bosch process [28].

In the Haber-Bosch process, N₂ is converted to NH₃ to Equation 1. This process requires high temperatures (>350-550 K) to enable the activation of the inert N₂ triple bond, while high pressures (>300 atm) are concomitantly needed to drive this overall exergonic reaction forward.



In contrast to the extreme conditions required in the Haber-Bosch process, biological nitrogen fixation takes place under ambient conditions, albeit at the expense of 16 ATP molecules in each catalytic cycle (Equation 2).



To overcome the high kinetic and thermodynamic stability of N₂, nitrogenase employs an exquisitely complex, but incompletely understood choreography of electron transfer (ET) and proton transfer (PT) processes.

The most widely distributed nitrogenase is Mo-containing nitrogenase (Figure 1A) [12]. It consists of two protein components, the molybdenum-iron protein (MoFeP) and the iron-protein (FeP). MoFeP is an (αβ)₂ dimer of dimers and contains two unique metal clusters, the catalytic iron-molybdenum cofactor FeMoco, a [7Fe:9S:1Mo:1C] cluster, and the P-cluster with the composition of [8Fe:7S]. FeP is a γ₂ homodimer harboring a [4Fe:4S] cluster at the dimer interface and two ATP binding sites [49, 57] (Figure 1).

As shown in Equation 2, each enzymatic turnover reaction by nitrogenase is an 8-e⁻ process. These electrons are delivered one at a time to MoFeP by FeP, with two ATP molecules consumed by FeP for each electron transferred [33, 57]. FeP is the only known biological agent that can reduce MoFeP and activate it for catalysis. In turn, MoFeP is the only protein that can support ATP hydrolysis by FeP. These observations underscore the importance of specific ATP-dependent interactions between these two proteins and implies the presence of conformationally gated redox events (see sections 1.2 and 1.3). Electrons donated by FeP are first received by the P-cluster and then relayed to FeMoco, which reduces substrates in a stepwise fashion (Figure 2) [29, 33, 36, 57, 68].

1.2 Evidence for gated-ET in nitrogenase

Alongside the enigmatic process of N₂ reduction by FeMoco, the mechanism of ATP-driven ET events within the FeP-MoFeP complex remains one of the key questions in biological nitrogen fixation. While the structural basis for how MoFeP docking activates ATP

hydrolysis by FeP is relatively well understood [56, 62] (Section 1.3), the mechanism of how FeP induces conformational changes within MoFeP is not (Section 2). Compared to other biological redox systems, FeP and MoFeP possess several distinguishing features. First, FeP differs from common electron shuttles such as flavodoxins, ferredoxins and cytochromes by its large size and in its requirement to bind and hydrolyze ATP during ET. ATP-dependent docking interactions between FeP and MoFeP involve the formation of unusually large interfaces [49, 62], which are more typical of permanent rather than transient protein complexes. Because of these extensive interactions, FeP dissociates from MoFeP very slowly, with an estimated rate of 6-10 s⁻¹ [37, 44, 68]. It is postulated that the unusually long lifetime of the FeP-MoFeP complex may be necessary for the orchestration of gated redox events within MoFeP [61]. Several other lines of evidence support conformationally controlled ET within the nitrogenase complex [29, 33, 57]:

1. The rate of ET between FeP and MoFeP is dependent on the osmolarity of the solution, implying a conformational rearrangement of the FeP-MoFeP complex is required prior to interprotein ET [10].
2. The order of ET appears to be (i) slow transfer between P-cluster and FeMoco and (ii) rapid “backfill” from the P-cluster to the FeP [4Fe:4S] [9], suggesting that the conformational gating likely involves ET from P-cluster to FeMoco.
3. Potent, low-potential photosensitizers, placed in close proximity to P-cluster, are not able to support efficient catalysis when illuminated with light, likely due to the fact that MoFeP conformations populated during ET events in catalysis cannot be accessed in absence of FeP [52, 53].

These combined findings paint a picture in which reduced, ATP-bound FeP binds MoFeP, and induces conformational changes within MoFeP to activate ET between P-cluster and FeMoco [29, 33].

1.3 Structural dynamics of the FeP-MoFeP complex

The crystal structures of several FeP-MoFeP complexes (from *Azotobacter vinelandii*) have been obtained under conditions relevant for ATP hydrolysis and catalytic turnover (Figure 3) [49, 62]. These structures reveal that FeP adopts at least three distinct, nucleotide-state dependent docking geometries (DG) (Figure 3). In DG1, FeP largely docks with the β -subunit surface of MoFeP (Encounter complex in Figure 3) [44, 66, 67], forming a complex that is stabilized predominantly by electrostatic interactions between negatively charged FeP residues γ 110-112, and positively charged MoFeP residues β 399-401 [44, 62]. In this geometry, the [4Fe:4S] of FeP is positioned >20 Å away from the P-cluster, suggesting that this conformation is not active for interprotein ET. At the same time, several lines of evidence suggests that the DG1 complex is a functionally relevant initial encounter complex whose mechanistic role is to increase the rate of association between FeP and MoFeP during turnover, especially when FeP/MoFeP ratios are low [44][64]. Indeed, that the elimination of favorable H-bonding and electrostatic interactions between FeP and MoFeP through point mutations such as β Lys400Glu and β Arg401Glu leads to considerable reduction of the catalytic activity of MoFeP [44].

DG2 represents the ATP-activated state of the nitrogenase complex and has been obtained in the presence of the non-hydrolyzable ATP analog AMPPCP or ADP.AIF₄⁻, the transition-state analog for ATP hydrolysis (Figure 3). In DG2, FeP is centrally located atop the αβ-interface surface of MoFeP, allowing the [4Fe:4S] to approach the P-cluster as closely as physically possible, yielding an ET-conductive distance of ~15 Å [62][56][8]. At the same time, FeP adopts a compact structure (particularly in the ADP.AIF₄⁻-bound form) that enables residues on each FeP subunit to extend across the dimer interface to participate in the hydrolysis of the bound nucleotide in the adjacent subunit. In DG2, the interface between FeP and MoFeP is particularly large (>3700 Å²), which allows the FeP to adopt undergo nucleotide-state-dependent conformational changes while retaining its central position on the MoFeP surface. Interestingly, one of the crystallographically characterized DG2 complexes is obtained in the presence of equimolar AMPPCP and ADP, with the two nucleotides bound asymmetrically by the FeP subunits (AMPPCP/ADP complex in Figure 3) [61]. This binding mode suggests that ATP hydrolysis and phosphate release within DG2 may proceed by a stepwise, rather than a concerted mechanism. Such a stepwise mechanism could be expected to prolong the lifetime of the activated FeP-MoFeP complex and, in turn, could orchestrate the sequence of intracomplex ET required for substrate reduction through the associated Fe-protein conformational changes [59].

Finally, DG3 is obtained in the presence of ADP, and may represent a FeP-MoFeP conformation that is populated after ET and ATP hydrolysis have taken place within DG2 (Figure 3) [62]. In DG3, the ADP-bound FeP is found in a relaxed conformation typical of uncomplexed FeP variants, and interacts primarily with the α-subunit surface of MoFeP. Like in the DG1 complex, the distance of >20 Å between the [4Fe:4S] cluster and the P-cluster is prohibitively long for ET. The mechanistic relevance of DG3 has yet to be probed experimentally through structure/function studies.

Taken together, these crystallographic snapshots suggest that FeP explores an unusually large conformational space along the MoFeP surface during ATP hydrolysis, whereby distinct docking geometries are selectively populated, depending on the Fe-protein nucleotide state. This allows the distance between the [4Fe:4S] and the P-clusters to be directly coupled to the nucleotide state, providing a way for actively modulating electron flow in nitrogenase. Interestingly, the correlation between the nucleotide state and the docking positions of FeP suggests that irreversible ATP hydrolysis may serve as a ratchet that provides directionality to protein-protein interactions, much in the same way that ATP hydrolysis ensures directed motion in proteins such as AAA⁺ domains [27, 47] and helicase [20]. Yet, none of the FeP-MoFeP complex structures offers any clues about the nature of the proposed redox-gating mechanism *within* MoFeP that could control ET between the P-cluster and FeMoco: in these complexes, MoFeP displays no structural changes near the P-cluster, FeMoco or the intervening region between these clusters suggestive of a gating process.

1.4. Redox-dependent structural changes in the P-cluster of *A. vinelandii* MoFe-protein

A survey of all available MoFeP crystal structures (uncomplexed or complexed with FeP) reveals that the only notable conformational change observed on the ET pathway to FeMoco

is on the P-cluster itself. It was established that the dithionite (DT)-reduced, all-ferrous P cluster (P^N) could be reversibly oxidized by one and two electrons to P^{+1} and P^{OX} states, respectively [7, 31, 57]. As demonstrated by a crystal structure of the *A. vinelandii* MoFeP (*Av*-MoFeP) [46], the oxidation of the P-cluster leads to a dramatic structural rearrangement: in the P^N state, the P-cluster can be viewed as a fusion of two closed [4Fe:4S] cubane architectures joined by a shared hexacoordinate sulfide, S1 (Figure 4). In the P^{OX} state, one of the cubane units opens up, whereby Fe5 bonds to the backbone amide N of *Av*- α Cys88, Fe6 ligates to *Av*- β Ser188, and Fe5 and Fe6 dissociate from S1. Since both the α -Cys88 backbone N and the β -Ser188 hydroxyl group likely have to be deprotonated to coordinate Fe ions, they would stabilize the P-cluster in an oxidized state, thus lowering its reduction potential and enabling it to deliver electrons to FeMoco. Therefore, any structural perturbation induced by FeP-MoFeP association that favors ligation by *Av*- β S188 and the *Av*- α C88 backbone N would provide a basis for the conformational redox gating in nitrogenase.

To determine if redox-dependent structural changes in the P-cluster are conserved, and thus likely to be important, we searched genomic databases and literature to find nitrogenases that showed sequence variations in residues that are proximal to the P-cluster, in particular positions equivalent to *Av*- β Ser188. We limited our search to organisms with fully sequenced genomes and only considered bacterial species that could be readily cultured in a laboratory. Based on these criteria, we concluded that the diazotroph *Gluconacetobacter diazotrophicus* (*Gd*) represents a promising model organism for studying nitrogenase.

1.5. Redox-dependent structural changes in the P-cluster of *G. diazotrophicus* MoFe-protein

Most of our structural and mechanistic understanding on enzymatic nitrogen fixation has been obtained through the study of nitrogenases from a small number of diazotrophic bacteria: *A. vinelandii*, *Klebsiella pneumonia* (*Kp*), and *Clostridium pasteurianum* (*Cp*). *A. vinelandii* and *K. pneumonia* are closely related γ -proteobacteria, and express group 1 nitrogenases [30, 48] that are structurally and functionally very similar to one another [13-15, 36, 38, 63, 68]. *Cp*-nitrogenase is structurally slightly dissimilar in the α -subunit [70] and is classified as a group 2 nitrogenase [30, 48]. Nevertheless, these three structurally well characterized nitrogenases feature the same cofactor architecture and there is little sequence or structural variability in functionally critical regions of the enzyme. To gain information on the conformational gating mechanism, we decided to investigate a nitrogenase with sequence differences compared to nitrogenase from the aforementioned species. Based on the assumption that important mechanistic features of an enzyme will be conserved even if the amino acid sequence is not, we set out to investigate nitrogenase from *Gd*-nitrogenase.

G. diazotrophicus harbors a group 1 nitrogenase like *Av*-nitrogenase. *Gd*- and *Av*-nitrogenases share 60% sequence identity. However, *Gd*-nitrogenase exhibits key amino acid sequence differences surrounding the P-cluster. *Gd*-MoFeP features an Ala (*Gd*- β Ala187) at the equivalent position to *Av*- β Ser188 (Table 1) and a Tyr residue at the position equivalent to *Av*- β Phe99 (*Gd*- β Tyr98). Interestingly, analysis of class 1 nitrogenase sequences indicates

that in the great majority of type 1 nitrogenases, the aforementioned amino acid pairs Ser/Phe and Ala/Tyr are covariant [30]: if MoFeP has a Ser in the first position, it features a Phe in the second. If an organism has an Ala in the first position, it has a Tyr in the second.

To investigate whether this two-position covariance has a functional significance and if *Gd*-MoFeP P-cluster can undergo similar redox-dependent structural changes as its *Av* counterpart, we expressed and isolated *Gd*-MoFeP protein and solved its crystal structure in P^N and P^{OX} states at 1.8 and 2.6 Å resolution, respectively [43]. As expected from their high sequence homologies, the overall architecture of *Gd*-MoFeP is very similar to that of *Av*-MoFeP with an RMSD of 0.7 Å over all ÅC atoms (Figure 1B). The coordination and the secondary-sphere environments of FeMoco are identical to one another in both species. Furthermore, in the P^N state, *Av*-P-cluster and (*Gd*-P-cluster are fully superimposable (Figure 4).

In contrast, the P^{OX} form of the *Gd*-MoFeP P-cluster displays striking differences from its *Av*-MoFeP counterpart, as shown in Figure 4 and Table 2. Analogous to structural changes observed in *Av*-MoFeP, Fe5 becomes ligated to the backbone N of *Gd*-αCys104 and dissociates from the central S1 upon P-cluster oxidation. However, Ser, which coordinates Fe6 in *Av*-, *Kp*-, and *Cp*-MoFeP, is replaced by Ala in *Gd*-MoFeP. Instead, Fe8 now coordinates the O atom of the *Gd*-βTyr98 side chain. Tyr-ligated Fe8 also fully dissociates from S1 like the Ser-coordinated Fe6 in other species. Thus, while 2-e⁻ oxidation of the P-clusters in both *Gd*- and *Av*-MoFeP yields an opened 4Fe-3S unit with two O- and N-based ligands, the mechanism by which this is achieved is distinct in these species.

While ligation of a Ser or Tyr to an FeS cluster is rare [40], the role of an O-based ligand as a redox switch for an FeS-cluster can be readily explained. Coordination by the singly anionic tyrosinate (Tyr⁻) or serinate (Ser⁻) side chains would decrease the reduction potential of the P-cluster to induce ET to FeMoco, much like a cysteinate (Cys⁻) ligand. However, unlike the borderline soft Cys⁻ ligand, the coordination of the hard Tyr⁻ and Ser⁻ ligands to an FeS-cluster would be highly dependent on whether the Fe center that they coordinate to is in the +3 (hard, favored) or +2 (borderline soft, disfavored) oxidation state. In other words, while Cys⁻ is a good permanent ligand that can stably anchor an Fe-S cluster in all oxidation states, Tyr⁻ and Ser⁻ are conditionally labile ligands that are well suited for reversible redox switching.

Our findings strongly suggest that redox-dependent structural changes at P-cluster are conserved and therefore likely relevant for nitrogenase function. Furthermore, the fact that P-cluster can cycle between the P^N and P^{OX} state through the engagement of conserved structural features hints at the possibility that it may be capable of transferring two electrons to FeMoco during catalytic turnover. Such 2-e⁻ transfer steps between P-cluster and FeMoco may help minimize wasteful H⁺ reduction during turnover by increasing the electron flux to FeMoco [33, 43]. Nevertheless, the functional importance of the P^{OX} state has yet to be experimentally established, as only P^N and P⁺¹ have been detected under catalytic turnover conditions.[34]Likewise, the mechanism by which FeP-MoFeP interactions can induce conformational changes in the P-cluster at a distance of >15 Å and modulate its coordination-dependent redox equilibria also remains an exciting topic for future studies.

2. Methods

The methods presented herein describe how to efficiently culture *G. diazotrophicus* in large scale for the expression of *Gd*-nitrogenase component proteins. These procedures are based on protocols first introduced by Fisher and Newton [22], and then adopted and modified by us [43]. For more detailed information on factors influencing *G. diazotrophicus* growth, readers are directed to Reis *et al.* [50], Flores-Encarnacion *et al.* [23], and Tejera *et al.* [60]. We furthermore present methods on the crystallographic and spectroscopic (EPR) characterization of *Gd*-MoFeP.

2.1 *G. diazotrophicus* as a model nitrogen-fixing organism

G. diazotrophicus is a gram-negative α -proteobacterium that was first isolated from sugarcane in Brazil [6]. It is an endophyte that establishes symbiosis with its host by infecting the host plant's roots where it colonizes intercellular spaces [55]. Unlike the other nitrogenase model organisms *A. vinelandii*, *K. pneumoniae*, and *C. pasteranum*, *G. diazotrophicus* is an agriculturally important species due to its plant growth enhancing properties which have been documented in several crops, including sugar cane, coffee and rice [45, 55, 58]. The economic potential of *G. diazotrophicus* is highlighted by the fact that it is often included in "biofertilizer" products, which contain a variety of plant growth promoting, beneficial bacteria.

The entire genome *G. diazotrophicus* has been sequenced and it indicates that the organization of its nitrogen fixing genes resembles that of other proteobacteria such as *A. vinelandii* [3, 24, 35]. *Gd*-nitrogenase is part of the *nif* operon, which contains the genes for FeP, both MoFeP subunits, and several accessory proteins (Figure 5).

2.2 Equipment and reagents

2.2.1 Major equipment and instruments needed

Anaerobic chamber (<i>e.g.</i> Coy glovebag)
Crystal trays and crystallography tools
Liquid nitrogen
Fast protein liquid chromatography (FPLC) workstation
Gas chromatograph with FID detector
Gastight syringes (multiple sizes from 0.025–1 mL)
Large capacity shaker, (<i>e.g.</i> , Amerex 767, New Brunswick Excella E25)
Large capacity Erlenmeyer (6 L) or Fernbach (2.8 L) flasks
Large round bottom flasks (1.5–3 L) to hold buffers with adaptors to connect to Schlenk line and FPLC
Microfluidizer
Peak shaped flasks (5 mL, 10 mL, 200 mL, and 500 mL) for loading protein onto FPLC
Schlenk line
Stoppered 10 or 14-mL glass serum vials (Wheaton)

2.2.2 Reagents required for the growth of *G. diazotrophicus*

Metal salts

CaCl₂·2H₂O

FeSO₄·7H₂O

MgSO₄·7H₂O

Na₂MoO₄·2H₂O

Sugar

Glucose

Sucrose

Buffer

K₂HPO₄

KH₂PO₄

Nitrogen source

(NH₄)₂SO₄

NH₄Cl

C2 media components

Peptone

NaCl

Yeast extract

Agar (for solid media only)

Indicators

Bromophenol blue

Bromothymol blue

2.2.3 Reagents required for nitrogenase purification, enzymatic assays and crystallization.

Nitrogenase purification

NaCl

Tris base

Sodium dithionite (DT)

Enzymatic assays

ATP (as Na₂ATP)

Creatine phosphate

Creatine phosphatase

Glacial acetic acid to quench reaction

MgCl₂

Concentration measurement

Urea

2,2-bipyridine

Crystallography
2-methyl-2,4-pentanediol (MPD)
Indigo sulfonate (indigo carmine, IDS)
Sodium cacodylate
Spermine
Zwittergent

2.3 *G. diazotrophicus* growth media

G. diazotrophicus is grown in LGI media for nitrogenase expression. To maintain cell stocks, LGI, LGIP or C2 media can be used (Figures 6 and 7).

1. LGI contains 10% glucose 0.14 mM CaCl₂, 0.81 mM MgSO₄, 0.036 mM FeSO₄, 0.008 mM NaMo₂O₄, 0.5 mM (NH₄)₂SO₄ or 1 mM NH₄Cl, 10 mM KPO₄ at pH 6.0.
2. LGIP can be used as an alternative to LGI for cell culture maintenance. LGIP uses the same recipe as LGI with the exception that sucrose is used instead of glucose. We do not recommend using LGIP for nitrogenase expression since the amount of nitrogenase produced is higher when using LGI, an observation that can be attributed to the higher respiration rate of *G. diazotrophicus* when glucose is used as the carbon source [60].
3. To make solid media, agar is added to a concentration of 12 g/L.
4. We observed that while growing *G. diazotrophicus* in absence of any fixed nitrogen is possible on solid media (Figure 6), doing so in liquid media results in impractically long lag phases. Therefore, 0.5 mM (NH₄)₂SO₄ or 1 mM NH₄Cl is added to liquid media (Figure 7). If high-level nitrogenase expression is not the primary goal, more NH₄⁺ (up to a concentration of 10 mM) can be added to increase the bacterial growth rate (Figure 7).
5. C2 media is made by mixing 10 g peptone, 15 g glucose, 5 g NaCl, and 5 g yeast extract per L.

For the improved visualization of cell colonies on solid media, pH indicators (bromothymol blue or bromphenol blue) can be added to the media. During growth, *G. diazotrophicus* secretes organic acids, which cause the pH of growth media to decrease from 6.0 to 2.5-3.5 (Figure 6) and a concomitant change in indicator color. Per L of solid media, 5 mL of indicator is added from a 0.5% solution dissolved in 0.5 N KOH.

2.4 *G. diazotrophicus* freezer stocks

C2 is a rich medium used to grow *G. diazotrophicus* for cell stock maintenance and to make freezer stocks.

1. Starting with a single colony from C2 or an LGI agar plate, start a 100-mL culture in a 500-mL Erlenmeyer flask. Cultures are grown in an orbital shaker, with a speed of 200 rpm at 30 °C.

2. To make a freezer stock, grow *G. diazotrophicus* to late exponential phase such that OD_{660nm} is ca. 1.0.
3. Spin down the cells, at 2000 × g for 15 min.
4. Resuspend the cells gently in 1/20th of the original volume in LGI supplemented with 20 mg/L yeast extract and 20% (v/v) glycerol.
5. Freeze the cells in liquid N₂ and store at –80°C.

2.5 Nitrogenase expression in *G. diazotrophicus*

2.5.1 General growth considerations—To date, no heterologous expression system exists for nitrogenase production in high yields. Although it is possible to express both FeP and MoFeP in *E. coli* [5] and MoFeP in yeast [65], expression levels are very low and not suitable for large scale biochemical and structural investigations. Therefore, nitrogenase is produced in the native host organism under the control of its native promoter. To induce nitrogenase expression in *G. diazotrophicus*, cells are cultured in LGI media containing 1 mM NH₄⁺, which is added to allow *G. diazotrophicus* to grow rapidly until mid-exponential phase, where the bacteria run out of fixed nitrogen. After NH₄⁺ is depleted, *G. diazotrophicus* starts transcribing the *nif* operon and reducing N₂ (Figure 7) [26].

To obtain sufficient quantities of protein required for protein crystallography, we found that growth of multiple medium-sized batches of *G. diazotrophicus* cultures (10-12 L) in 6 L Erlenmeyer or 2.8 L Fernbach flasks works quite well. While it was reported that large-volume fermenters can be used for nitrogenase expression in *G. diazotrophicus* [22], we found that the protein yields from flask-grown cultures are superior to those of grown in fermenters (60 L, in our case).

2.5.2 Factors affecting nitrogenase expression in *G. diazotrophicus*—The levels of nitrogenase expression in *G. diazotrophicus* are affected by aeration, the type of carbon source and the concentration of sugar (carbon source) in the medium [23, 50]. To maximize the yield of *Gd*-nitrogenase, bacteria are grown in LGI media containing 10% (w/v) glucose. *G. diazotrophicus*, is an obligate aerobe, and high aeration rates are necessary to meet the bacterium's respiratory needs under N₂ fixing conditions [23]. Optimal aeration conditions for nitrogenase expression in *G. diazotrophicus* entail agitation at 200 rpm in an orbital shaker, with Erlenmeyer flasks containing 0.4 L of media per L flask volume, or Fernbach flasks filled with 0.55 L of media per L flask volume. We found that lower or higher rates of aeration negatively affects nitrogenase yields.

1. Starting with a freezer stock, prepare a 200-mL LGI starter culture and grow the culture until the cells reach late exponential or early stationary phase. The cell density at this point should be between 1.5–2 at 660 nm.
2. To start large-scale growth, inoculate LGI with 20 mL/L of starter culture.
3. Monitor cell growth by measuring OD_{660nm} and measure nitrogenase expression by observing C₂H₂ reduction (Figure 7 and section 3.5.3).

4. Nitrogenase expression is first observed after 2-3 days when OD_{660nm} ranges between 1 and 1.5.
5. Peak nitrogenase activity is approximately 40-80 nmol C₂H₄ per 1 mL of cell culture (Figure 7).
6. After detecting C₂H₂ reduction, grow *G. diazotrophicus* for an additional 2-4 hrs. During this period, monitor C₂H₂ reduction every 1 h.
7. Harvest *G. diazotrophicus* by centrifugation at 2000 × *g* for 15 min. Typical *G. diazotrophicus* yield is 2.5 g per L of LGI.
8. The cell pellet may be stored indefinitely at -80°C.

2.5.3 Monitoring nitrogenase activity in whole cells

1. Place 1 mL of cells in a stoppered serum vial and add C₂H₂ to a pressure of 0.072 atm. This step is done by transferring C₂H₂ from a previously degassed round bottom flask filled with C₂H₂ to the stoppered vial filled using a gastight syringe.
2. Place the cells in a shaking water bath set to 30°C, and incubate them for 10-15 min.
3. *G. diazotrophicus* expressing nitrogenase reduces C₂H₂ to C₂H₄. C₂H₂ and C₂H₄ can be separated by GC on an alumina column and detected using an FID detector.

2.6 Buffers and solutions for *G. diazotrophicus* lysis and nitrogenase purification

Protein purification	
Resuspension, lysis, and wash buffer (Buffer R)	50 mM Tris (pH 8), 100 mM NaCl, 5 mM DT
Elution buffer (Buffer E)	50 mM Tris (pH 8), 500 mM NaCl, 5 mM DT
Gel filtration buffer (Buffer GF)	50 mM Tris (pH 8), 500 mM NaCl, 5 mM DT
Activity assay	
Buffer A	50 mM Tris (pH 8), 5 mM MgCl ₂ , 5 mM ATP, 5 mM ATP, 30 mM creatine phosphate, 0.125 mg/mL creatine phosphatase
Buffer B	0.5 M Tris base
Buffer C	50 mM Tris (pH 8), 500 mM NaCl
Protein concentration measurement	
Urea	8 M
Bipyridine	100 mM in 50% glacial acetic acid

2.7 *G. diazotrophicus* lysis and nitrogenase purification

2.7.1 General procedures for working with nitrogenase: Nitrogenase components are highly air sensitive. *Gd*-nitrogenase is manipulated using anaerobic methods on a Schlenk line and in an anaerobic chamber at O₂ levels below 5 ppm. All buffers and

equipment are degassed and, unless specifically indicated. DT is added to a concentration of 5 mM to maintain a reducing environment.

2.7.2 Lysis

1. Thaw *G. diazotrophicus* on ice.
2. Resuspend *G. diazotrophicus* in chilled Buffer R. Add 3 mL of buffer per g of cells. It is important to keep all solutions cool during lysis to avoid heat denaturation of *Gd-FeP*. Prior to lysis, add DT to a final concentration of 5 mM.

Neither osmotic lysis methods nor sonication efficiently lyse *G. diazotrophicus* cells, so we prefer using a microfluidizer. The exact protocol of cell lysis will be dependent on the specific hardware. We use an LM10 instrument fitted with an F12Y interaction chamber (Microfluidics Corporation) to lyse *G. diazotrophicus* at 16,000 – 18,000 psi. Typically, 3 passes are needed to fully lyse the entire cell pellet. To avoid oxygen damage to nitrogenase, lysis is carried out under a blanket of Ar.

1. Place the cell lysate in an airtight centrifuge bottle equipped with a rubber septum and degass the solution for a total of 20 min on a Schlenk line by repeatedly exchanging the headspace with Ar.
2. Clarify the cell lysate by centrifugation at $17500 \times g$ for 1 hr. During centrifugation, the supernatant may darken slightly.
3. After clarification, transfer the supernatant to a pear-shaped flask in an anaerobic chamber (Figure 8A).

2.7.3 Purification

1. Load the clarified lysate onto an DEAE column pre-equilibrated with anaerobic buffer R. Use ca. 7.5 mL of DEAE resin per g of cell paste.
2. Wash the column with fresh Buffer E until the flowthrough is clear.
3. Elute *Gd-MoFeP* and *Gd-FeP* using a 100 – 500 mM linear NaCl gradient. *Gd-MoFeP* and *Gd-FeP* co-elute between 250 and 300 mM NaCl (Figure 8B).
4. Determine the presence and purity of *Gd-MoFeP* and *Gd-FeP* by SDS-PAGE. *Gd-MoFeP* and *Gd-FeP* mostly co-elute and there is no benefit to separating *Gd-MoFeP* and *Gd-FeP* fractions at this stage.
5. Pool *Gd-FeP/Gd-MoFeP* fractions, concentrate the resulting solution to 5-10 mL in an anaerobic chamber, and load it onto a Superdex 200 gel filtration column equilibrated with anaerobic Buffer GF. The gel filtration column removes remaining impurities from *Gd-MoFeP* and *Gd-FeP* and separates the proteins from each other (Figure 8C). The major impurity is a ferredoxin (ca. 8 kDa), which elutes after both *Gd-nitrogenase* components.
6. Use SDS-PAGE to identify proteins contained in each collected fraction.
7. Typical *Gd-MoFeP* yields are 2-4 mg protein per L of cell culture (0.08-0.2 mg *Gd-MoFeP* per g of cell pellet).

8. Pool and concentrate the respective fractions of *Gd*-FeP and *Gd*-MoFeP and run an SDS-PAGE to evaluate the purity of the respective proteins (Figure 8D).
9. Measure the concentration of the respective proteins using the Bradford assay [4] and by measuring the protein's respective Fe content. For the later assay, mix 10-20 μL of protein with 780-790 μL of 8 M urea and 100 μL of 0.1 M bipyridine. Let the sample incubate for 5 min and determine the Fe concentration using $\epsilon_{522\text{nm}} = 8650 \text{ M}^{-1}\text{cm}^{-1}$.
10. Purified proteins can be stored in liquid nitrogen indefinitely.

2.8 *Gd*-nitrogenase activity assays

The activity of *Gd*-nitrogenase is measured according to previously described protocols for C_2H_2 reduction [22, 43, 44]. Experiments are conducted under an Ar atmosphere in stoppered serum vials containing a buffered activity assay solution of 50 mM Tris (pH 8), 60 mM NaCl, 5 mM ATP, 5 mM MgCl_2 , 30 mM creatine phosphate, 0.125 mg/mL creatine phosphokinase, and 13 mM DT.

1. Mix the appropriate amounts of Buffer A and Buffer C in serum vials to make the activity assay solution. The total volume of a typical reaction in our experiments is typically ~ 1.1 mL. The amount of Buffer C that needs to be added to Buffer A will vary depending on the volume of *Gd*-MoFeP and *Gd*-FeP that is added in steps 5 and 6.
2. Degas 2 mL of Buffer B in a stoppered serum vial and use it to anaerobically dissolve DT to a final concentration of 0.5 M.
3. Degas the serum vials containing the activity assay solution and add DT to a final concentration of 13 mM using a gastight syringe.
4. Add C_2H_2 to each serum vial to a final pressure of 0.072 atm using a gastight syringe.
5. Add *Gd*-MoFeP, suspended in buffer C, to final concentration of 0.2 μM to each serum vials using a gastight syringe.
6. To initiate the reaction, anaerobically add increasing amounts of *Gd*-FeP, suspended in buffer C, to final concentrations ranging between 0-12 μM using a gastight syringe.
7. Incubate the reaction for 10 min at 30 $^\circ\text{C}$ in a shaking water bath.
8. Terminate the reaction by adding 0.3 mL of glacial acetic acid.
9. C_2H_2 and C_2H_4 can be separated by GC using an alumina column and detected using a flame-ionization detector.

The specific C_2H_2 reduction activity of *Gd*-MoFeP ranges between 1000 and 1500 $\text{nmol mg}^{-1}\text{min}^{-1}$.

2.9 Electron paramagnetic resonance (EPR) spectroscopy

EPR spectroscopy is a powerful method to monitor and characterize different redox states of the P-cluster and FeMoco. In the perpendicular collection mode, DT-reduced MoFeP displays signals at $g \sim 4.3$, 3.6, and 2.0, arising from the resting-state ($S=3/2$) FeMoco (termed M^N) [31]. Under these conditions, the all-ferrous P-cluster (*i.e.*, P^N) is EPR-silent in both parallel and perpendicular modes. In the $2-e^-$ oxidized P^{OX} state, the P-cluster features a diamagnetic $S = 3$ non-Kramers doublet with a signal at large g -values ($g = 12$ in *Av*-MoFeP, $g = 16$ in *Gd*-MoFeP) [31], observable in parallel collection mode. For more information on EPR spectroscopy of nitrogenase, the reader is directed to reviews by Igarashi and Seefeldt [31] and Danylak *et al.* [11].

1. Set up EPR experiments using protein concentrations of $50 \mu\text{M}$ in an anaerobic chamber.
2. To generate P^N , add DT to a concentration of 5 mM to *Gd*-MoFeP and incubate for 5 min. Place the protein in an EPR tube and seal the tube.
3. For P^{OX} samples, first remove any DT by running MoFeP over a desalting column (*e.g.*, 10DG from GE Healthcare) prior to adding IDS. Then, add IDS to *Gd*-MoFeP a final concentration of 0.42 mM.
4. Flash freeze P^N and P^{OX} samples in liquid N_2 .
5. All EPR experiments are carried out at 10 K.
6. Collect perpendicular-mode spectra on an X-band EPR spectrometer using the following settings: microwave frequency; 9.64 GHz, modulation frequency; 100.00 Hz, modulation amplitude; 10.02, microwave power; 6.4 mW, attenuation; 15.0 dB, time constant; 81.92 msec, conversion time; 40.96 msec.

DT-reduced *Gd*-MoFeP features a signal for FeMoco in the M^N state with peaks at $g = 4.3$, 3.6, and 2.0 (Figure 9).

1. Collect parallel-mode spectra on an X-band EPR spectrometer using the following settings: Microwave frequency; 9.36 GHz, modulation frequency; 100.00 Hz, modulation amplitude; 10.02, microwave power; 6.4 mW, attenuation; 15.0 dB, time constant; 81.92 msec, conversion time; 40.96 msec.

IDS-oxidized *Gd*-MoFeP features a signal at $g = 16.0$ in the parallel collection mode, indicative of $2-e^-$ oxidized P-cluster with $S = 3$ (Figure 9). In perpendicular mode, the signal of DT-reduced and IDS-oxidized *Gd*-MoFeP are identical since no change in the FeMoco oxidation state occurs [43].

1. To obtain high signal-to-noise spectra, collect at least 20 scans per sample.

Since EPR spectroscopy is a non-destructive technique, protein can be removed from the EPR tube and used for subsequent experiments. Furthermore, redox-dependent changes in the P-cluster are reversible. MoFeP in the P^{OX} state can be reduced by addition of excess DT, and MoFeP in the P^N state can be oxidized by addition of excess IDS.

2.10 *Gd*-MoFeP crystallization and data collection

2.10.1 Crystallization—Several successful methods and conditions for MoFeP crystallization have been developed. For a thorough review on nitrogenase crystallography, we direct the reader to a review by Roth and Tezcan [54]. To crystallize *Gd*-MoFeP, we chose to set up crystallization trials in a 24-well sitting drop format. The general format of the tray uses a solution of sodium 0.1 M cacodylate (pH 6.5), 40–50% MPD, and 0.2–0.6 M NaCl.

1. Place a stereomicroscope in the anaerobic chamber to be able to view crystals without removing the crystal trays from the chamber.
2. Crystallization of DT-reduced *Gd*-nitrogenase: Grow crystals anaerobically using the sitting drop method with a *Gd*-MoFeP concentration of ca. 170 μ M (40 mg/mL). The well solution contains 45% MPD, 300 mM NaCl, 100 mM sodium cacodylate (pH 6.5), 1 mM spermine, 0.1% Zwittergent, and 5 mM Na₂S₂O₄. The drop consists of 2 μ L *Gd*-MoFeP in a buffered solution of 25 mM Tris (pH 8), 100 mM NaCl, and 2 μ L of well solution.
3. Crystallization of IDS-oxidized *Gd*-nitrogenase: To obtain oxidized *Gd*-MoFeP crystals, 2 μ L of *Gd*-MoFeP (170 μ M) is mixed with 2 μ L of well solution containing of 50% MPD, 300 mM NaCl, 100 mM sodium cacodylate (pH 6.5), 1 mM spermine, and 0.43 mM IDS. IDS is added from a 42 mM stock, which is spun at 12000 $\times g$ prior to use to remove undissolved IDS.

For both reduced and oxidized *Gd*-MoFeP, the best diffracting crystals were obtained with 45–50% MPD, however, we recommend using a broader range of MPD concentrations (40–55% in initial screens. While the inclusion of NaCl led to the highest quality crystals, we also observed diffraction-quality crystals when NaCl was replaced with KCl. Similarly, high-quality crystals were found both in presence and absence of Zwittergent and spermine. To find best diffracting crystals, we recommend adjusting the concentration of spermine between 0 and 1 mM in a fine screen.

The crystal morphology is identical in both redox conditions. *Gd*-MoFeP crystals appear as rectangular rods with dimensions varying between approximately 0.04 and 0.4 mm. Crystals start to appear within 24 h, with additional crystals forming for up to 1 week.

1. *Gd*-MoFeP crystals are harvested aerobically and flash frozen in liquid N₂. At 40–50%, MPD itself acts a glassing agent so no additional cryoprotectants are needed. To prevent oxygen damage during crystal harvesting, unseal only one well at a time, and complete harvesting within 5 min per tray. To further reduce oxygen damage and to keep the crystals anaerobic, harvesting can be carried out under a stream of inert gas.

2.10.2 Data collection, data processing and structural refinement—Diffraction experiments are carried out at a synchrotron or a home source, where the experimental strategy needs to be optimized for the respective hardware. Multiple free and commercially available indexing and integrating options are available today, including XDS [32],

HKL2000 [42], and imosflm [2]. Aimless [21] can be used for scaling and merging, and Ctruncate [21] to convert structure factors to amplitudes.

2.10.3 Structural refinement—The structure of *Gd*-MoFeP can be solved by molecular replacement, using the structure of *Av*-MoFeP can be used as the search model. We recommend removing metal clusters from the search model. Phasing can be carried out using freely available software, including PhaserMR [1] and Molrep [69]. The structure can be refined automatically using remlcp [39], phenix.refine [1] and manually in coot [19].

To build the metal clusters, start with manual refinement.

1. Load P-cluster and FeMoco from an existing structure into the *Gd*-MoFeP in Coot [18] and move the respective clusters into electron density map, simultaneously using either the $2F_o-F_c$ and F_o-F_c map. Then, merge the clusters with the polypeptide.
2. After initial cluster placement, move the individual cluster atoms manually until they fit the electron density map.

Geometry constraints are necessary for automated refinement of the FeMoco and P-cluster. The respective constraint file contains coordinates and geometry information for each metal cluster. The files include values for each bond length, bond angle, and torsion (dihedral) angle in the respective cluster, as well as the maximum allowed deviation for each of the values. For both P-cluster and FeMoco, the maximum allowed deviation is 0.020 Å for bond distances, 3° for bond angles, and 20° for torsion angles. Making a new constraint file is necessary whenever the structure that needs to be refined differs substantially from one used to build the original constraint file. Since the structures of FeMoco and P^N in *Gd*-MoFeP closely resemble those in *Av*-MoFeP, existing constraint files originally generated for *Av*-MoFeP can be used. In this case, automated refinement will accurately place the atoms of the metal clusters into the electron density map and little additional manual refinement is needed.

The structure of P^{OX} in *Gd*-FeMoco, however, features large structural changes involving Fe6 and Fe8 that differ from *Av*-MoFeP P^{OX}. Therefore, oxidized *Gd*-MoFeP requires a new constraint file for P^{OX}. To make a new constraint file, the protein structure is first opened in Coot and the P-cluster is manually re-built by moving Fe and S ions until all cluster atoms fit the $2F_c-F_c$ electron density map. After fully placing the cluster, distances, bond angles, and torsion angles between cluster atoms are measured in Coot or in Pymol (Schrödinger). The values for respective distances and angles are input into a text editor according to cif format guidelines [25] to create a new constraint file. The text file can be saved as a “.cif” file that is recognized as a constraint file by remlcp and phenix.refine.

3. Conclusion

Here we have summarized recent studies on the ATP- and oxidation-state dependent structural dynamics of nitrogenase and the insights gained in these studies. Our investigations were greatly augmented by the examination of nitrogenase component proteins from a new model organism *G. diazotrophicus*. To afford easy access to similar

investigations, we have also described methods to isolate and characterize *Gd*-MoFeP. We hope that the relatively straightforward expression, purification and crystallization of *Gd*-MoFeP encourages readers to rediscover a lost interest in the study of nitrogenases from different diazotrophic bacteria [16, 17]. Thanks to advances in bioinformatics, researchers have conducted detailed sequence analyses of known nitrogenases and uncovered amino acid variances in mechanistically critical regions of the protein, including selenocysteine ligation to P-cluster and amino acid variability in the outer coordination sphere of FeMoco [30]. We anticipate that the growing pool of genome sequences from diazotrophic bacteria will greatly augment the biochemical and structural investigation of the nitrogenase mechanism and possibly lead to the discovery of nitrogenases with novel chemistries.

Acknowledgements

This work was supported by NIH (GM099813 to F.A.T.). F.A.T. also acknowledges the Frasch Foundation for further support. C.P.O. gratefully acknowledges support by USDA NIFA (Grant 2015-67012-22895). The authors also thank Michael Medina for his contributions and useful discussion.

Abbreviations

ATP	Adenosine triphosphate
<i>Av</i>	<i>Azotobacter vinelandii</i>
<i>Cp</i>	<i>Clostridium pasteurianum</i>
DG	Docking geometry
DT	Sodium dithionite
EPR	Electron paramagnetic resonance
ET	Electron transfer
FeP	Iron protein
FPLC	Fast protein liquid chromatography
<i>Gd</i>	<i>Gluconacetobacter diazotrophicus</i>
IDS	Indigo carmine (5,5'-indigodisulfonic acid)
<i>Kp</i>	<i>Klebsiella pneumoniae</i>
MoFeP	Molybdenum iron protein
MPD	2-methyl-2,4-pentanediol
RMSD	Root mean square deviation
TRIS	2-amino-2-hydroxymethylpropane-1,3-diol
SDS-PAGE	Sodium dodecyl sulfate polyacrylamide gel electrophoresis

References

- [1]. Adams PD , Afonine PV , Bunkóczi G , Chen VB , Davis IW , Echols N , Headd JJ , Hung LW , Kapral GJ , Grosse-Kunstleve RW , McCoy AJ , Moriarty NW , Oeffner R , Read RJ , Richardson DC , Richardson JS , Terwilliger TC , Zwart PH (2010). PHENIX: a comprehensive Python-based system for macromolecular structure solution. *Acta Crystallographica. Section D, Biological Crystallography*, 66, 213–221. [PubMed: 20124702]
- [2]. Battye TG , Kontogiannis L , Johnson O , Powell HR , Leslie AG (2011). iMOSFLM: a new graphical interface for diffraction-image processing with MOSFLM. *Acta Crystallographica. Section D, Biological Crystallography*, 67, 271–81. [PubMed: 21460445]
- [3]. Bertalan M , Albano R , de Pádua V , Rouws L , Rojas C , Hemerly A , Teixeira K , Schwab S , Araujo J , Oliveira A (2009). Complete genome sequence of the sugarcane nitrogen-fixing endophyte *Gluconacetobacter diazotrophicus* Pal5. *BMC Genomics*, 10, 450. [PubMed: 19775431]
- [4]. Bradford MM (1976). A rapid and sensitive method for the quantitation of microgram quantities of protein utilizing the principle of protein-dye binding. *Analytical Biochemistry*, 72, 248–254. [PubMed: 942051]
- [5]. Buren S , Young EM , Sweeny EA , Lopez-Torres G , Veldhuizen M , Voigt CA , Rubio LM (2017). Formation of Nitrogenase NifDK Tetramers in the Mitochondria of *Saccharomyces cerevisiae* ACS Synthetic Biology, in press, printed online 03/03/2017.
- [6]. Cavalcante VA , Dobereiner J (1988). A new acid-tolerant nitrogen-fixing bacterium associated with sugarcane. *Plant and Soil*, 108, 22–31.
- [7]. Chan JM , Christiansen J , Dean DR , Seefeldt LC (1999). Spectroscopic evidence for changes in the redox state of the nitrogenase P-cluster during turnover. *Biochemistry*, 38, 5779–5785. [PubMed: 10231529]
- [8]. Chiu H , Peters JW , Lanzilotta WN , Ryle MJ , Seefeldt LC , Howard JB , Rees DC (2001). MgATP-Bound and nucleotide-free structures of a nitrogenase protein complex between the Leu 127 Delta-Fe-protein and the MoFe-protein. *Biochemistry*, 40, 641–50. [PubMed: 11170380]
- [9]. Danyl K , Dean DR , Hoffman BM , Seefeldt LC (2011). Electron transfer within nitrogenase: evidence for a deficit-spending mechanism. *Biochemistry*, 50, 9255–9263. [PubMed: 21939270]
- [10]. Danyl K , Mayweather D , Dean DR , Seefeldt LC , Hoffman BM (2010). Conformational gating of electron transfer from the nitrogenase Fe protein to MoFe protein. *Journal of the American Chemical Society*, 132, 6894–6895. [PubMed: 20429505]
- [11]. Danyl K , Yang ZY , Seefeldt LC (2011). Electron paramagnetic resonance spectroscopy. *Methods in Molecular Biology*, 766, 191–205. [PubMed: 21833869]
- [12]. Dos Santos PC , Fang Z , Mason SW , Setubal JC , Dixon R (2012). Distribution of nitrogen fixation and nitrogenase-like sequences amongst microbial genomes. *BMC Genomics*, 13, 162. [PubMed: 22554235]
- [13]. Duyvis MG , Wassink H , Haaker H (1998). Nitrogenase of *Azotobacter vinelandii*: kinetic analysis of the Fe protein redox cycle. *Biochemistry*, 37, 17345–17354. [PubMed: 9860849]
- [14]. Duyvis MG , Wassink H , Haaker H (1996). Pre-steady-state kinetics of nitrogenase from *Azotobacter vinelandii*. Evidence for an ATP-induced conformational change of the nitrogenase complex as part of the reaction mechanism. *The Journal of Biological Chemistry*, 271, 29632–29636. [PubMed: 8939894]
- [15]. Einsle O , Tezcan FA , Andrade SL , Schmid B , Yoshida M , Howard JB , Rees DC (2002). Nitrogenase MoFe-protein at 1.16 Å resolution: a central ligand in the FeMo-cofactor. *Science*, 297, 1696–1700. [PubMed: 12215645]
- [16]. Emerich DW , Burris RH (1978). Nitrogenase from *Bacillus polymyxa*. Purification and properties of the component proteins. *Biochimica et Biophysica Acta*, 536, 172–183. [PubMed: 213121]
- [17]. Emerich DW , Burris RH (1978). Preparation of nitrogenase. *Methods in Enzymology*, 53, 314–29. [PubMed: 101737]
- [18]. Emsley P , Cowtan K (2004). Coot: model-building tools for molecular graphics. *Acta Crystallographica. Section D, Biological Crystallography*, 60, 2126–2132. [PubMed: 15572765]

- [19]. Emsley P , Lohkamp B , Scott WG , Cowtan K (2010). Features and development of Coot. *Acta Crystallographica. Section D, Biological Crystallography*, 66, 486–501. [PubMed: 20383002]
- [20]. Enemark EJ , Joshua-Tor L (2008). On helicases and other motor proteins. *Current Opinions in Structural Biology*, 18, 243–57.
- [21]. Evans PR , Murshudov GN (2013). How good are my data and what is the resolution? *Acta Crystallographica. Section D, Biological Crystallography*, 69, 1204–14. [PubMed: 23793146]
- [22]. Fisher K , Newton WE (2005). Nitrogenase proteins from *Gluconacetobacter diazotrophicus*, a sugarcane-colonizing bacterium. *Biochimica et Biophysica Acta*, 1750, 154–165. [PubMed: 15925553]
- [23]. Flores-Encarnacion M , Contreras-Zentella M , Soto-Urzuza L , Aguilar GR , Baca BE , Escamilla JE (1999). The respiratory system and diazotrophic activity of *Acetobacter diazotrophicus* PAL5. *Journal of Bacteriology*, 181, 6987–95. [PubMed: 10559164]
- [24]. Giongo A , Tyler HL , Zipperer UN , Triplett EW (2010). Two genome sequences of the same bacterial strain, *Gluconacetobacter diazotrophicus* PAI 5, suggest a new standard in genome sequence submission. *Standards in Genomic Sciences*, 2, 309–317. [PubMed: 21304715]
- [25]. Hall SR , Allen FH , Brown ID (1991). The Crystallographic Information File (CIF): A New Standard Archive File for Crystallography. *Acta Crystallographica*, A47, 655–685.
- [26]. Hamilton TL , Jacobson M , Ludwig M , Boyd ES , Bryant DA , Dean DR , Peters JW (2011). Differential accumulation of *nif* structural gene mRNA in *Azotobacter vinelandii*. *Journal of Bacteriology*, 193, 4534–6. [PubMed: 21725008]
- [27]. Hanson PI , Whiteheart SW (2005). AAA+ proteins: have engine, will work. *Nat Rev Molecular and Cellular Biology*, 6, 519–29. [PubMed: 16072036]
- [28]. Hirsch PR , Mauchline TH (2015). The Importance of the Microbial N Cycle in Soil for Crop Plant Nutrition. *Advances in Applied Microbiology*, 93, 45–71. [PubMed: 26505688]
- [29]. Hoffman BM , Lukoyanov D , Yang Z-Y , Dean DR , Seefeldt LC (2014). Mechanism of nitrogen fixation by nitrogenase: the next stage. *Chemical Reviews*, 114, 4041–4062. [PubMed: 24467365]
- [30]. Howard JB , Kechris KJ , Rees DC , Glazer AN (2013). Multiple amino acid sequence alignment nitrogenase component 1: Insights into phylogenetics and structure-function relationships. *PLoS One*, 8, e72751. [PubMed: 24019874]
- [31]. Igarashi RY , Seefeldt LC (2003). Nitrogen fixation: the mechanism of the Mo-dependent nitrogenase. *Critical Reviews in Biochemistry and Molecular Biology*, 38, 351–384. [PubMed: 14551236]
- [32]. Kabsch W (2010). Integration, scaling, space-group assignment and post-refinement. *Acta Crystallographica. Section D, Biological Crystallography*, 66, 133–44. [PubMed: 20124693]
- [33]. Katz FEH , Owens CP , Tezcan FA (2016). Electron Transfer Reactions in Biological Nitrogen Fixation. *Israel Journal of Chemistry*, 56, 682–692.
- [34]. Lanzilotta WN , Christiansen J , Dean DR , Seefeldt LC (1998). Evidence for coupled electron and proton transfer in the [8Fe-7S] cluster of nitrogenase. *Biochemistry*, 37, 11376–11384. [PubMed: 9698385]
- [35]. Lee S , Reth A , Meletzus D , Sevilla M , Kennedy C (2000). Characterization of a major cluster of *nif*, *fix*, and associated genes in a sugarcane endophyte, *Acetobacter diazotrophicus*. *Journal of Bacteriology*, 182, 7088–7091. [PubMed: 11092875]
- [36]. Lowe D , Thorneley R (1984). The mechanism of *Klebsiella pneumoniae* nitrogenase action. Pre-steady-state kinetics of H₂ formation. *Biochemical Journal*, 224, 877–886. [PubMed: 6395861]
- [37]. Lowe DJ , Thorneley RN (1984). The mechanism of *Klebsiella pneumoniae* nitrogenase action. Pre-steady-state kinetics of H₂ formation. *Biochemical Journal*, 224, 877–886. [PubMed: 6395861]
- [38]. Mayer SM , Lawson DM , Gormal CA , Roe SM , Smith BE (1999). New insights into structure-function relationships in nitrogenase: a 1.6 Å resolution X-ray crystallographic study of *Klebsiella pneumoniae* MoFe-protein. *Journal of Molecular Biology*, 292, 871–891. [PubMed: 10525412]

- [39]. Murshudov GN , Vagin AA , Dodson EJ (1997). Refinement of macromolecular structures by the maximum-likelihood method. *Acta Crystallographica. Section D, Biological Crystallography*, 53, 240–55. [PubMed: 15299926]
- [40]. Nicolet Y , Rohac R , Martin L , Fontecilla-Camps JC (2013). X-ray snapshots of possible intermediates in the time course of synthesis and degradation of protein-bound Fe₄S₄ clusters. *Proceedings of the National Academies of Sciences of the United States of America*, 110, 7188–92.
- [41]. Oldroyd GED , Dixon R (2014). Biotechnological solutions to the nitrogen problem. *Current Opinion in Biotechnology*, 26, 19–24. [PubMed: 24679253]
- [42]. Otwinowski Z , Minor W (1997). Processing of X-ray diffraction data collected in oscillation mode. *Methods in Enzymology*, 276, 307–26.
- [43]. Owens CP , Katz FE , Carter CH , Oswald VF , Tezcan FA (2016). Tyrosine-Coordinated P-Cluster in *G. diazotrophicus* Nitrogenase: Evidence for the Importance of O-Based Ligands in Conformationally Gated Electron Transfer. *Journal of the American Chemical Society*, 138, 10124–7. [PubMed: 27487256]
- [44]. Owens CP , Katz FEH , Carter CH , Luca MA , Tezcan FA (2015). Evidence for functionally relevant encounter complexes in nitrogenase catalysis. *Journal of the American Chemical Society*, 137, 12704–12712. [PubMed: 26360912]
- [45]. Pedraza RO (2008). Recent advances in nitrogen-fixing acetic acid bacteria. *International Journal of Food Microbiology*, 125, 25–35. [PubMed: 18177965]
- [46]. Peters JW , Stowell MH , Soltis SM , Finnegan MG , Johnson MK , Rees DC (1997). Redox-dependent structural changes in the nitrogenase P-cluster. *Biochemistry*, 36, 1181–1187. [PubMed: 9063865]
- [47]. Rappas M , Bose D , Zhang X (2007). Bacterial enhancer-binding proteins: unlocking sigma54-dependent gene transcription. *Current Opinions in Structural Biology*, 17, 110–6.
- [48]. Raymond J , Siefert JL , Staples CR , Blankenship RE (2004). The natural history of nitrogen fixation. *Molecular Biology and Evolution*, 21, 541–54. [PubMed: 14694078]
- [49]. Rees DC , Akif Tezcan F , Haynes CA , Walton MY , Andrade S , Einsle O , Howard JB (2005). Structural basis of biological nitrogen fixation. *Philosophical Transactions of the Royal Society A: Mathematical, Physical and Engineering Sciences*, 363, 971–984.
- [50]. Reis VM , Döbereiner J (1998). Effect of high sugar concentration on nitrogenase activity of *Acetobacter diazotrophicus*. *Archives of Microbiology*, 171, 13–18. [PubMed: 9871014]
- [51]. Rogers C , Oldroyd GE (2014). Synthetic biology approaches to engineering the nitrogen symbiosis in cereals. *Journal of Experimental Botany*, 65, 1939–46. [PubMed: 24687978]
- [52]. Roth LE , Nguyen JC , Tezcan FA (2010). ATP- and iron-protein-independent activation of nitrogenase catalysis by light. *Journal of the American Chemical Society*, 132, 13672–13674. [PubMed: 20843032]
- [53]. Roth LE , Tezcan FA (2012). ATP-uncoupled, six-electron photoreduction of hydrogen cyanide to methane by the molybdenum-iron protein. *Journal of the American Chemical Society*, 134, 8416–8419. [PubMed: 22564208]
- [54]. Roth LE , Tezcan FA (2011). X-ray crystallography. *Methods in Molecular Biology (Clifton, N.J.)*, 766, 147–164.
- [55]. Saravanan VS , Madhaiyan M , Osborne J , Thangaraju M , Sa TM (2008). Ecological occurrence of *Gluconacetobacter diazotrophicus* and nitrogen-fixing *Acetobacteraceae* members: their possible role in plant growth promotion. *Microbial Ecology*, 55, 130–140. [PubMed: 17574542]
- [56]. Schindelin H , Kisker C , Schlessman JL , Howard JB , Rees DC (1997). Structure of ADP x AIF₄(-)-stabilized nitrogenase complex and its implications for signal transduction. *Nature*, 387, 370–376. [PubMed: 9163420]
- [57]. Seefeldt LC , Hoffman BM , Dean DR (2009). Mechanism of Mo-dependent nitrogenase. *Annual Review of Biochemistry*, 78, 701–722.
- [58]. Sevilla M , Burris RH , Gunapala N , Kennedy C (2001). Comparison of benefit to sugarcane plant growth and ¹⁵N₂ incorporation following inoculation of sterile plants with *Acetobacter diazotrophicus* wild-type and Nif- mutants strains. *Molecular Plant-Microbe Interactions : MPMI*, 14, 358–366. [PubMed: 11277433]

- [59]. Spatzal T , Perez KA , Einsle O , Howard JB , Rees DC (2014). Ligand binding to the FeMo-cofactor: Structures of CO-bound and reactivated nitrogenase. *Science*, 345, 1620–1623. [PubMed: 25258081]
- [60]. Tejera NA , Ortega E , Rodes R , Lluch C (2004). Influence of carbon and nitrogen sources on growth, nitrogenase activity, and carbon metabolism of *Gluconacetobacter diazotrophicus*. *Canadian Journal of Microbiology*, 50, 745–50. [PubMed: 15644929]
- [61]. Tezcan FA , Kaiser JT , Howard JB , Rees DC (2015). Structural evidence for asymmetrical nucleotide interactions in nitrogenase. *Journal of the American Chemical Society*, 137, 146–149. [PubMed: 25522159]
- [62]. Tezcan FA , Kaiser JT , Mustafi D , Walton MY , Howard JB , Rees DC (2005). Nitrogenase complexes: multiple docking sites for a nucleotide switch protein. *Science (New York, N.Y.)*, 309, 1377–1380.
- [63]. Thorneley RN , Lowe DJ (1983). Nitrogenase of *Klebsiella pneumoniae*. Kinetics of the dissociation of oxidized iron protein from molybdenum-iron protein: identification of the rate-limiting step for substrate reduction. *Biochemical Journal*, 215, 393–403. [PubMed: 6316927]
- [64]. Ubbink M (2009). The courtship of proteins: understanding the encounter complex. *FEBS Letters*, 583, 1060–1066. [PubMed: 19275897]
- [65]. Wang L , Zhang L , Liu Z , Zhao D , Liu X , Zhang B , Xie J , Hong Y , Li P , Chen S , Dixon R , Li J (2013). A minimal nitrogen fixation gene cluster from *Paenibacillus* sp. WLY78 enables expression of active nitrogenase in *Escherichia coli*. *PLoS Genet*, 9, e1003865. [PubMed: 24146630]
- [66]. Willing A , Howard JB (1990). Cross-linking site in *Azotobacter vinelandii* complex. *The Journal of Biological Chemistry*, 265, 6596–6599. [PubMed: 2324093]
- [67]. Willing AH , Georgiadis MM , Rees DC , Howard JB (1989). Cross-linking of nitrogenase components. Structure and activity of the covalent complex. *The Journal of Biological Chemistry*, 264, 8499–8503. [PubMed: 2722786]
- [68]. Wilson PE , Nyborg AC , Watt GD (2001). Duplication and extension of the Thorneley and Lowe kinetic model for *Klebsiella pneumoniae* nitrogenase catalysis using a mathematica software platform. *Biophysical Chemistry*, 91, 281–304. [PubMed: 11551440]
- [69]. Winn MD , Ballard CC , Cowtan KD , Dodson EJ , Emsley P , Evans PR , Keegan RM , Krissinel EB , Leslie AG , McCoy A , McNicholas SJ , Murshudov GN , Pannu NS , Potterton EA , Powell HR , Read RJ , Vagin A , Wilson KS (2011). Overview of the CCP4 suite and current developments. *Acta Crystallographica. Section D, Biological Crystallography*, 67, 235–42. [PubMed: 21460441]
- [70]. Zhang LM , Morrison CN , Kaiser JT , Rees DC (2015). Nitrogenase MoFe protein from *Clostridium pasteurianum* at 1.08 Å resolution: comparison with the *Azotobacter vinelandii* MoFe protein. *Acta Crystallographica. Section D, Biological Crystallography*, 71, 274–82. [PubMed: 25664737]

Highlights

- Nitrogenase from *G. diazotrophicus* has been isolated and structurally characterized for the first time.
- The P-cluster of *G. diazotrophicus* MoFeP undergoes redox-dependent structural changes that are distinct from those of hitherto-characterized MoFeP variants from other organisms.
- The reversible ligation of the *G. diazotrophicus* P-cluster to a Tyr ligand strongly suggests the importance of hard, O-based ligands in mediating conformationally-gated electron transfer in nitrogenase

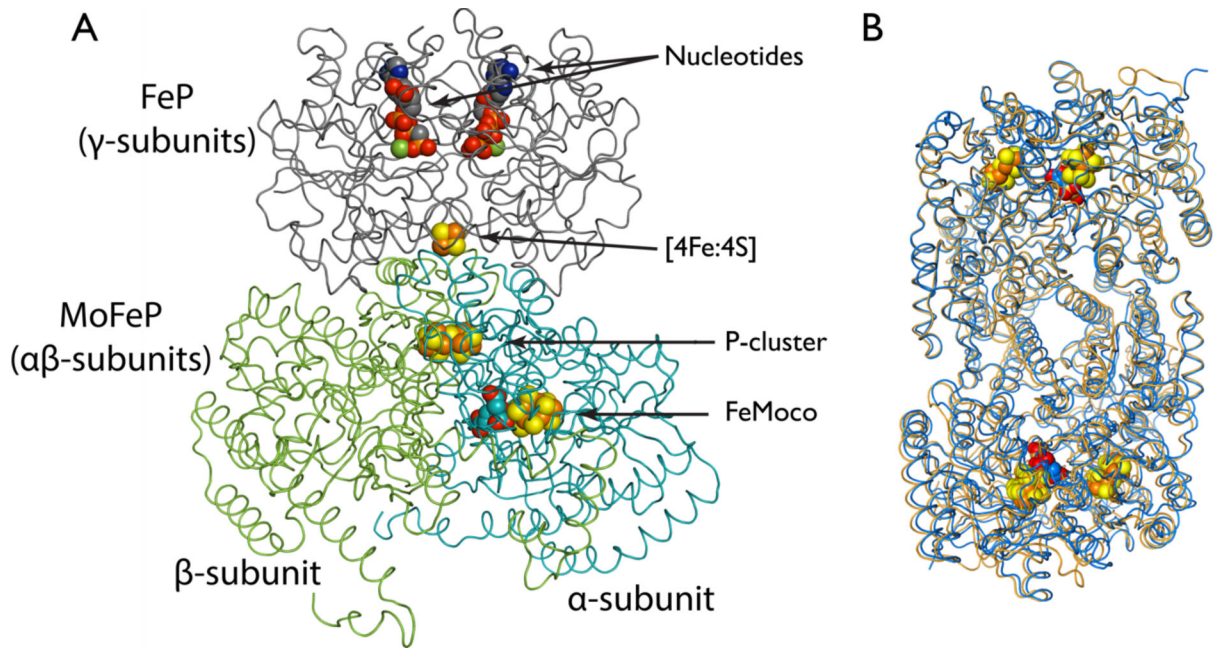


Figure 1.

(A) Structure of nitrogenase. For simplicity, only one half of the $(\alpha\beta)_2(\gamma_2)_2$ complex is shown. (B). Structural alignment of the entire $(\alpha\beta)_2$ MoFeP of *A. vinelandii* (orange) with that of *G. diazotrophicus* (blue), illustrating their structural similarity. Metal clusters and bound nucleotides are shown as spheres.

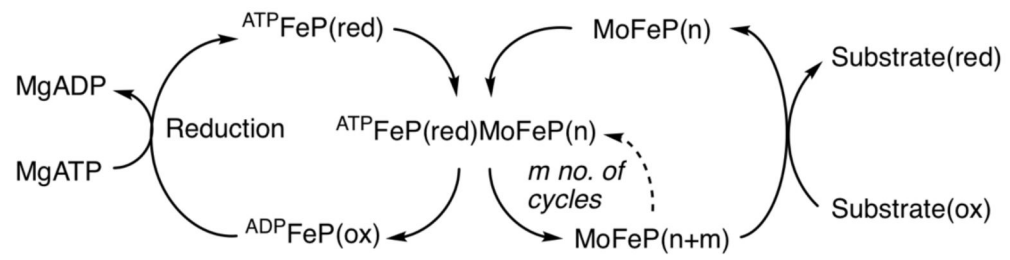


Figure 2.

Model for electron transfer and ATP hydrolysis during nitrogenase turnover. The number of cycles depends on the substrate, where $m = 8$ for N_2 and $m = 2$ for C_2H_2 and H^+ . The value (n) refers to the number of electrons accumulated on FeMoco.

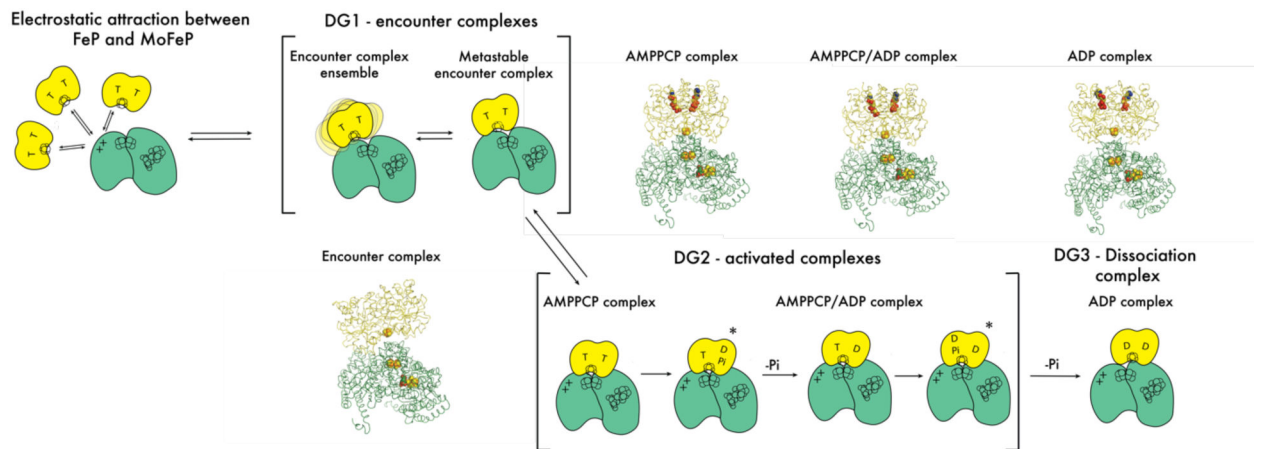


Figure 3.

Proposed scheme for nitrogenase turnover depicting ATP-dependent FeP-MoFeP interactions populated during turnover, where T represents ATP and D represent ADP. Conformations marked with an * are likely sub-states, but have not yet been experimentally observed. The structures of known turnover intermediates are depicted as cartoons.

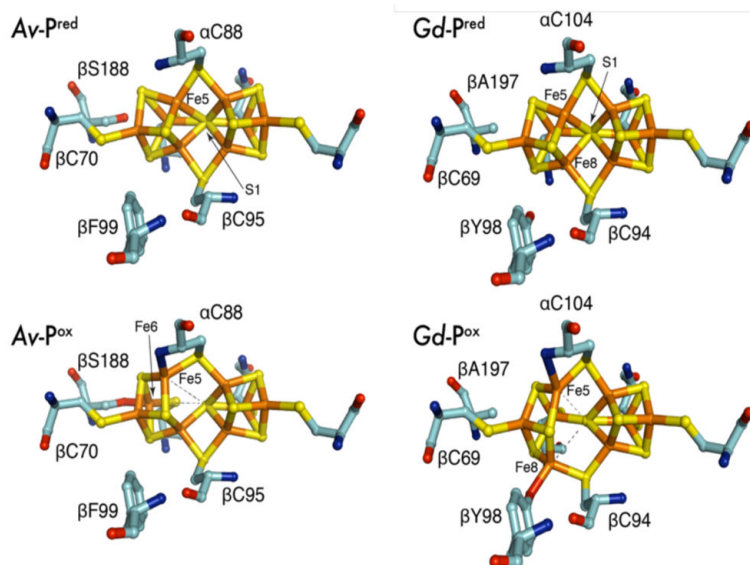


Figure 4. Redox-dependent structural changes in *Av*- and *Gd*-MoFeP. The dashed lines in P^{OX} highlight bonds to the central sulfide S1 that are broken upon oxidation.

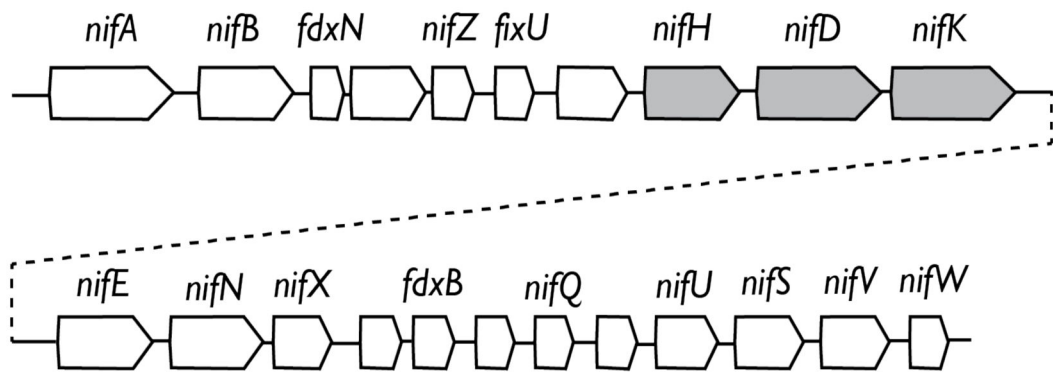


Figure 5.

Nif operon of *G. diazotrophicus*. *NifH* represent FeP, *nifD*, the α -subunit of MoFeP and *nifK* the β -subunit. For clarity, *nif* genes downstream of *nifW* (*fixA* – *modD*) are omitted.

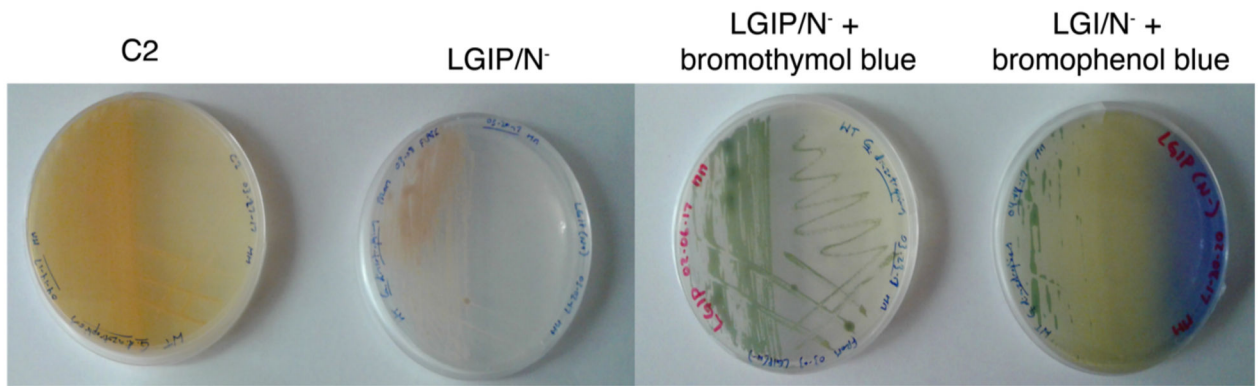


Figure 6.

G. diazotrophicus grown on different types of solid media. *G. diazotrophicus* grows to highest density on rich media (C2) compared to minimal, NH₄⁺-free media (LGIP and LGI). Both bromothymol blue and bromophenol blue can be used to better visualize bacteria. Bromothymol blue is taken up by the bacteria, where it is green at neutral pH. This provides contrast to media, where bromothymol blue is almost clear under acidic conditions. Bromophenol is blue-green when taken up by *G. diazotrophicus*. As *G. diazotrophicus* acidifies the surrounding media during growth, bromophenol blue in the media changes color from blue to yellow. This color change is useful for visualizing the extent of bacterial growth. When grown to full density, the LGI plate containing bromophenol blue should be almost completely yellow.

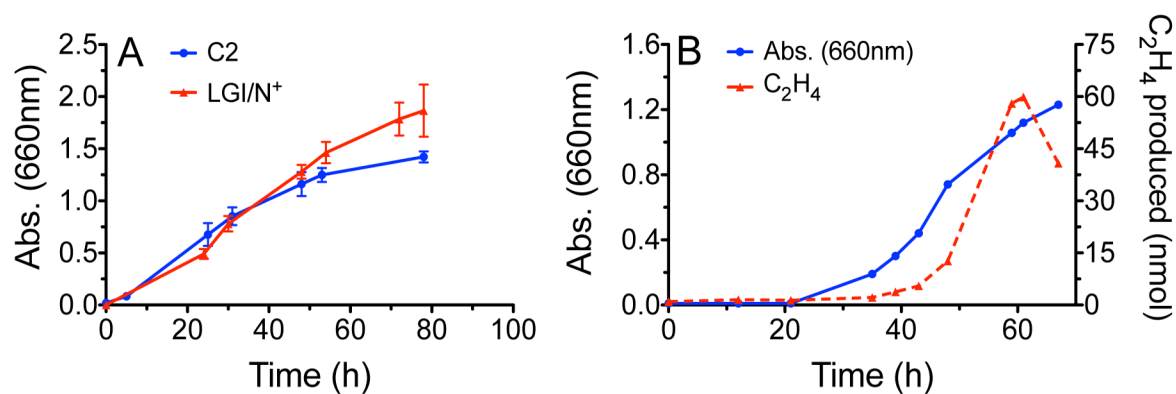


Figure 7.

(A) Growth curves for *G. diazotrophicus* grown in rich C2 and LGI/N⁺ (10 mM NH₄⁺) media. (B) Growth curves for *G. diazotrophicus* grown under N₂-fixing conditions. The growth medium contains 1 mM NH₄⁺. Nitrogenase expression is monitored by measuring reduction of the alternative substrate C₂H₂ to C₂H₄. Nitrogenase expression starts in mid-exponential phase (40 h) when NH₄⁺ originally present in the medium is depleted. It is important to continuously monitor C₂H₄ production since MoFeP expression decreases slightly once intracellular NH₄⁺ levels reach homostasis [26]. Note that the different durations of the lag phases in (A) and (B) are due to the fact that different amounts of starter cultures were used for inoculation.

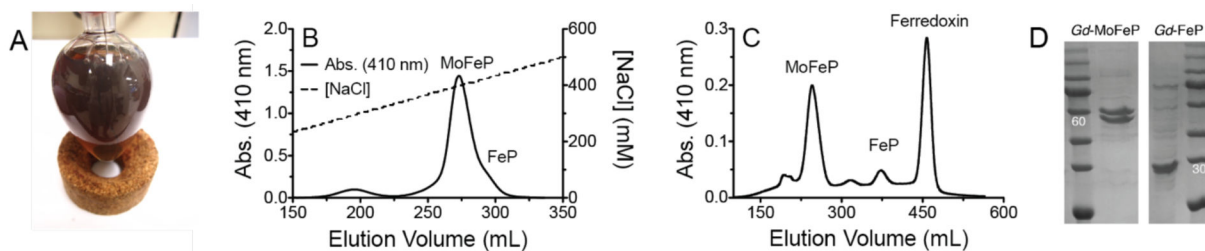


Figure 8.

(A) Clarified cell lysate collected in a pear-shaped flask. The brown color arises from the FeS clusters of MoFeP and FeP. (B) DEAE and (C) gel filtration chromatograms of *Gd*-nitrogenase. Note that in the ion exchange step, MoFeP and FeP co-elute. We do not recommend trying to separate the nitrogenase components in this step, since they are readily separated by gel filtration chromatography at a later stage. (D) SDS-PAGE of purified *Gd*-MoFeP and *Gd*-FeP with relevant molecular weight marker bands indicated. The double band for *Gd*-MoFeP arises from the α and β subunits.

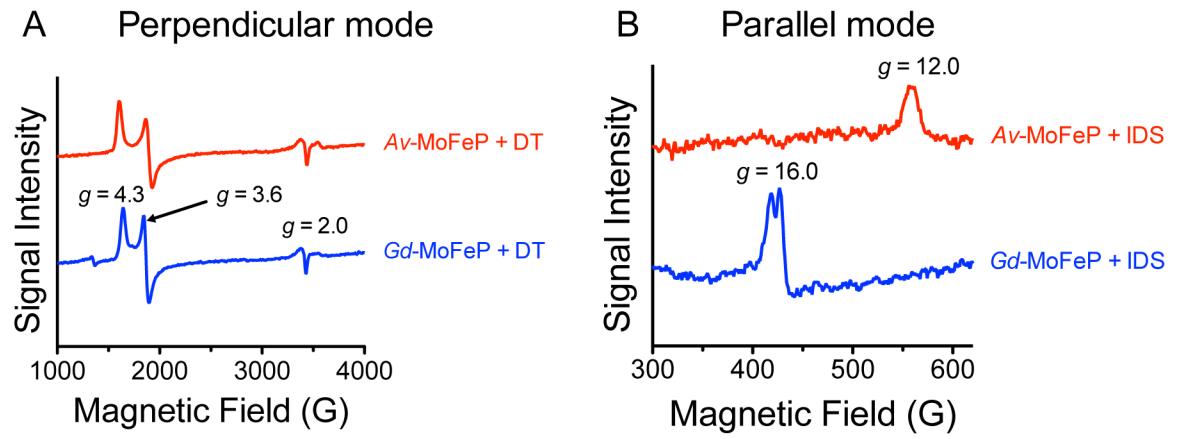


Figure 9. EPR spectra of *Gd-MoFeP*. The experimental conditions are described in the main text.

Table 1.

Sequence alignment of *Av*-, *Kp*-, *Cp*-, *Gd*-MoFeP illustrating sequence differences surrounding the P-cluster.

	<i>Av</i> - β 185-190	<i>Av</i> - β 95-100
<i>A. vinelandii</i>	HTPSFV	CVAYFR
<i>K. pneumoniae</i>	HTPSFI	CVAYFR
<i>C. pasteurianum</i>	NTPSYV	CCCYHR
<i>G. diazotrophicus</i>	HTPAFV	CVAYYR

Author Manuscript

Author Manuscript

Author Manuscript

Author Manuscript

Table 2.

Changes in coordination distances of the P-Cluster upon oxidation ($P^N \rightarrow P^{OX}$) in *A. vinelandii* and *G. diazotrophicus*.

	$d(S1-Fe6/Fe8)$ (Å)	$d(O^{ser/Tyr}-Fe6/Fe8)$ (Å)	$d(N^{Cys}-Fe5)$ (Å)
<i>Av-MoFeP</i>	2.5 → 4.0	3.4 → 1.9	3.4 → 2.1
<i>Cp-MoFeP</i>	2.4 → 3.6	3.2 → 2.0	3.3 → 2.3
<i>Kp-MoFeP</i>	2.4 → 3.8	3.6 → 2.2	3.4 → 2.2
<i>Gd-MoFeP</i>	2.5 → 3.4	3.6 → 2.1	3.4 → 2.6

Author Manuscript

Author Manuscript

Author Manuscript

Author Manuscript